Evaluation of novel reactive MgO activated slag binder for the immobilisation of lead and zinc

Fei Jin*, Abir Al-Tabbaa

Department of Engineering, University of Cambridge, Trumpington Road, Cambridge CB2 1PZ, UK

* Corresponding author: Fei Jin

Email: leonking1987@gmail.com

Tel: +44 1223 766683

Fax: +44 1223 339713

Address: Geotechnical Research Group, Engineering Department, Trumpington Road, Cambridge, UK, CB2 1PZ

Abstract: Although Portland cement is the most widely used binder in the stabilisation/solidification (S/S) processes, slag-based binders have gained significant attention recently due to their economic and environmental merits. In the present study, a novel binder, reactive MgO activated slag, is compared with hydrated lime activated slag in the immobilisation of lead and zinc. A series of lead or zinc-doped pastes and mortars were prepared with metal to binder ratio from 0.25% to 1%. The hydration products and microstructure were studied by X-ray diffraction, thermogravimetric analysis and scanning electron microscopy. The major hydration products were calcium silicate hydrate and hydrotalcite-like phases. The unconfined compressive strength was measured up to 160 d. Findings show that lead had a slight influence on the strength of MgO-slag paste while zinc reduced the strength significantly as its concentration increased. Leachate results using the TCLP tests revealed that the immobilisation degree was dependent on the pH and reactive MgO activated slag showed an increased pH buffering capacity, and thus improved the immobilisation efficiency compared to lime activated slag. It was proposed that zinc was mainly immobilised within the structure of the hydrotalcite-like phases or in the form of calcium zincate, while lead was primarily precipitated as the hydroxide. It is concluded, therefore, that reactive MgO activated slag can serve as clinker-free alternative binder in the S/S process.

Keywords: hydrated lime, reactive MgO, slag, hydrotalcite-like phases, lead/zinc immobilisation

1. Introduction

Stabilisation/Solidification (S/S) is a commonly used treatment method for heavy metal contamination which aims to improve the physical characteristics and to prevent the transport of the contaminants (Harbottle et al., 2007). These processes are based on various cementitious materials such as Portland cement (PC) and lime (Roy et al., 1991; Husillos Rodríguez et al., 2011). The hydration products of these binders not only physically encapsulate the waste material containing the heavy metals but also chemically react with the heavy metals to form complex compounds or simply precipitate them due to the high pH of the system (Spence and Shi, 2004). However, the production of PC is associated with intensive energy use and is reported to account for 5-8% of anthropogenic carbon emission (Scrivener and Kirkpatrick, 2008). Therefore, by-products such as ground granulated blast-furnace slag (GGBS) from iron production, or fly ash from coal-fired power stations, are commonly utilised to partially replace PC in the treatment process.

As a latent hydraulic cement, GGBS is often activated with PC, lime or other caustic alkalis. Numerous studies have focused on the performance of PC-slag or alkali-activated slag in the presence of lead or zinc, which are commonly encountered heavy metals in the contaminated soils and other wastes. In terms of strength development, Qian et al. (2003a, 2003b) studied zinc-doped waterglass activated slag (zinc/binder = 0.5 wt% and 2 wt%) and found that zinc decreased the strength significantly and this influence was dependent on the zinc concentration, which is consistent with Deja (2002), who studied the immobilisation of lead and zinc using waterglass activated slag and found zinc reduced the unconfined compressive strength (UCS) of the mortar by 20% (zinc/binder = 0.5% and 1%) while lead exhibited no observable influence on the strength after 2 yr (lead/binder = 1 wt% and 2 wt%). Hekal et al. (2012) found that lead retarded the early hydration of PC-slag due to the coating of calcium plumbate ($CaPbO_3 \bullet xH_2O$) on the cement particles, which is supported by Rha et al.

(2000). Nevertheless, Rha et al. (2000) also observed that after 7 d of curing, the strength of lead doped samples increased sharply and exceeded that of the control in the long term. As to the interference of heavy metals on the hydration process of PC or alkali activated slag, Hekal et al. (2012) found no formation of any new phases from XRD in the lead-doped PC-slag matrix. This is in agreement with Deja (2002) who detected no difference in terms of microstructure between control and contaminated (Zn or Pb) cement paste samples. Based on the analyses of hydration products, Qian et al. (2003a, 2003b) proposed three main fixation mechanisms for Zn in alkali-activated slag binder: (i) the formation of insoluble calcium zincate ($CaZn_2(OH)_6 \cdot 2H_2O$) precipitate; (ii) the formation of insoluble zinc silicate gel; and (iii) the incorporation of zinc within the lattice of calcium silicate hydrates (C-S-H), the main hydration product of PC. They also stated that the latter two mechanisms are preferable at low zinc concentration (< 0.5% by mass of slag) while excess zinc (2% by mass of slag) will precipitate as calcium zincate.

There is scarce research on the application of lime-slag binder for heavy metal immobilisation. Kogbara et al. (2011) investigated lime-slag binder used in soil stabilisation for various heavy metals such as Pb, Zn, Ni and Cd. They found that lime-slag and PC-slag binders could effectively reduce the leachability of the contaminants. In addition, the characteristics (e.g., strength, pH) of the cement-soil matrix were dependent on many variables such as water content, and binder dosage. However, no mineralogical or microstructure analysis was conducted regarding the hydration process of lime-slag in the presence of the heavy metals.

Reactive magnesia is usually calcined from magnesite/dolomite at a the temperature of ~1000 °C (compared to ~1450 °C for PC) and mainly contains MgO and minor levels of lime (CaO), quartz (SiO_2), magnesite ($MgCO_3$), dolomite ($MgCa(CO_3)_2$), and calcite ($CaCO_3$). Recently, reactive MgO emerged as an effective activator for slag (Yi et al., 2013;

Jin et al., 2013), the price of which is only slightly higher than that of lime or $Ca(OH)_2$, and similar to or cheaper than that of other alkaline reagents (Rötting et al., 2008). In addition, reactive MgO is a mild earth alkali, which is much easier to handle and transport, and has much less environmental impact compared to the caustic alkalis such as NaOH or waterglass. Yi et al. (2013) found that 10-20% MgO activated slag outperformed hydrated lime-activated slag paste in terms of long-term strength. Mineralogical analysis showed the main hydration products of reactive MgO and slag were C-S-H and hydrotalcite-like phases (Ht) (Yi et al., 2013; Jin et al., 2013). According to Hosni (2011), Ht has a general formula of $[M_{1-x}^{2+} M_x^{3+}(OH)_2][A_{x/n}^{n-} \bullet mH_2O]$, where M^{2+} represents a divalent metal, e.g., Mg, Mn, Fe, Co, Ni, Cu and Zn, M^{3+} represents a trivalent metal such as Al, Cr, and Fe and A is the interlayer anion, e.g., CO_3^{2-}, Cl^-, NO_3^-. The effectiveness of Ht as adsorbents for metals has been extensively investigated due to their natural anion exchange properties (Liang et al., 2013). It has been proved to be effectively removed lead and zinc in water (Rojas, 2013; Bankauskaite and Baltakys, 2014). In addition, the pore solution pH of reactive MgO-slag blends is in the range of 11-12.5 (Jin et al., 2013), which is much lower than the PC or alkali-activated slag (> 13) and this relative low pH could make it easier to form precipitates of metal hydroxides. All of the above mentioned characteristics render reactive MgO-slag cement as a potential sustainable and economical binder for heavy metal remediation. However, nothing is available in the literature on the performance of reactive MgO-slag cement in the immobilisation of heavy metals.

Hence, there are four objectives in the current study focussing on a comparison between reactive MgO and $Ca(OH)_2$ activated slag when doped with lead and zinc solutions in terms of: (i) strength; (ii) immobilisation efficiency; (iii) immobilisation mechanisms; and (iv) influence of the lead and zinc concentrations on the strength and hydration properties of the two binders. The hydration products were thoroughly characterised by various techniques

including thermogravimetric analysis (TGA), XRD and scanning electron microscopy (SEM). The immobilisation efficiency was evaluated by TCLP and the metal concentration was measured by inductively coupled plasma optical emission spectrometry (ICP-OES).

2. Materials and Methods

2.1. Binder materials and contaminants

Reactive MgO (M), obtained from Richard Baker Harrison, UK, and hydrated lime, i.e., $Ca(OH)_2$ (C) from Tarmac and Buxton Lime and Cement, UK, were used as the activators for a GGBS (G), obtained from Hanson, UK. The sharp sand, for use to produce a mortar, with D_{50} of 0.8 mm and coefficient of uniformity of 4.3, was obtained from Ridgeons, Cambridge, UK. The reactivity of the MgO is 100 s, measured by acetic acid test proposed in (Shand, 2006), classifying the MgO as of moderate reactivity (Jin and Al-Tabbaa, 2013). Table 1 presents the physico-chemical properties of the activators and GGBS used in the binder and the XRD patterns for the raw GGBS and reactive MgO are shown in Fig. 1. It can be seen that GGBS is featured by a broad peak around 25-35° assigned to the CaO-Al_2O_3-MgO-SiO_2 glass structure, while reactive MgO has characteristic peaks at 36.9, 38.4,42.9 and 44.4°. In addition, magnesite was not fully decomposed as manifested by the peak at ~32.6°, thought its content is < 5% as calculated from loss on ignition (Table 1). The lead and zinc were used as nitrate salts, obtained from Fisher Scientific, UK, and prepared as solutions using deionised water in the range of 0.25% to 1% by the weight of the binder.

2.2. Preparation of samples

A series of paste samples were prepared for the mineralogical, microstructural analysis and the leaching test while the corresponding mortar samples were used for determination of the UCS. The water to binder ratio was set as 0.4 for all the paste and mortar samples and the binder to sand ratio was 1:3 in the mortar samples. The quantity of the

activators (reactive MgO or $Ca(OH)_2$) used was 15% replacement of GGBS. To investigate the effect of lead and zinc on the hydration process of $Ca(OH)_2$/MgO-activated slag, the metal to binder ratio was varied from 0.25% to 1%. Table 2 presents the details of the mixes prepared.

Prior to mixing, the zinc nitrate and lead nitrate solutions were used as the mixing water to prepare the paste and mortar samples. The dry cement materials were firstly mixed in a bench-top food mixer to achieve homogeneity and the contaminated water was then added to the mix for a further mixing and homogenisation. The paste samples were cast into Ø 30×60 mm cylinders and the mortar samples were moulded into larger Ø 50×100 mm cylinders. After 24 h of curing in the moulds, the samples were demoulded and transferred into sealed plastic bags and cured at the temperature of 20±1 °C and relative humidity > 95% until ready for testing.

2.3. Testing methods

UCS of the mortar samples, was determined, in triplicate according to BS EN 196-1 (2005) at ages of 7, 28, 90 and 160 d. The paste samples were crushed to pass through the 1 mm sieve and TCLP leaching test (USEPA, 1992) was conducted in duplicate on samples cured for 7 and 28 d. In this procedure, 10 g of the specimen was weighed into a 250 mL polypropylene plastic bottle containing 200 mL dilute acetic acid with a pH of 2.88. The mixture was rotated for 24 h at a speed of 30 rpm and then filtered using a 0.45 µm membrane syringe filter after the pH measurement. The metal concentration in the filtered liquid was determined by Perkin Elmer 7000 ICP-OES instrument. The remaining specimen was stored in acetone to arrest the hydration and vacuum dried for at least 7 d to eliminate the acetone. Once dried, the specimen was ground to pass through a 75 µm sieve. TGA was conducted on PerkinElmer STA6000 equipment from 40 to 800 °C with the heating rate of

10 °C min^{-1}. XRD was carried out on the Siemens D5000 X-ray diffractometer using a scanning range from 5 to 60 (2θ), with a resolution of 0.05° per step and retention time of 1 s per step. SEM in combination with energy dispersive X-ray spectroscopy (EDS) was performed on the JEOL 5800LV machine.

3. Results and Discussion

3.1. Hydration products

3.1.1. XRD results

The XRD patterns of CG and MG series' pastes cured for 28 d are shown in Fig. 2. For both reference samples (CG and MG), poorly crystalline C-S-H was identified at 2θ ≈ 23.0, 26.6, 29.5, 31.3, and 49.8°. In addition, the characteristic peak of hydrotalcite-like phases (Ht) at 2θ ≈ 11.5° was also detected for all the mixes, which agrees well the findings of others on alkali-activated slags (Wang and Scrivener, 1995). Unreacted $Ca(OH)_2$ and MgO were identified suggesting that the slag hydration did not fully consume either activator at 28 d. It should be noted that no brucite was detected in MG series indicating that the consumption of brucite by slag hydration was faster than the MgO hydration rate, which is consistent with previous studies (Jin et al., 2013). In general, the presence of Pb or Zn did not significantly change the hydration phases in either system. Trace peaks for lead hydroxide and lead carbonated hydroxide hydrate were identified for pastes containing 1% Pb addition, indicating Pb was mainly precipitated as hydroxide and carbonated to some extent due to the exposure to air. On the other hand, Zn more easily reacted with Ca, as suggested in Qian et al. (2003b), so peaks for calcium zincate were detected. Note that peaks for lead hydroxide and calcium zincate overlap with those for C-S-H around 2θ ≈ 30°, hence, obscuring the identification of those phases by XRD.

The most remarkable difference between the contaminated samples and the reference is reflected at 2θ ≈ 10-12°. Numerous peaks were found due to the varying d-spacing of the Ht, which were attributed to the incorporation of anions between the layers such as CO_3^{2-} and NO_3^- from the salts used. For the MG series, low Zn (0.25%) contaminated samples appeared to have no effect on the phases formed (Fig. 2b). When Zn concentration increased to 1%, it was clear that the Ht peak totally shifted to a lower angle (larger d-spacing) suggesting more anions were fixed between the layers. Due to the similar size of zinc and magnesium atoms, when zinc nitrate was mixed with Ht, Zn easily substituted Mg in the structure of Ht (isomorphic substitution) (Liang et al., 2013). On the other hand, Pb is too large to be incorporated into the Ht structure and was hence mainly fixed by surface adsorption or precipitation, which was supported by Park et al. (2007) who studied the reaction between Pb and Mg/Al hydrotalcite.

3.1.2. TG results

The TG/DTG curves of CG and MG series' pastes cured for 28 d are shown in Fig. 3. From the TG curves, it was apparent that Zn-doped samples exhibited less total weight loss compared to the reference samples, indicating the retardation of the slag hydration, while Pb-doped samples showed approximately the same total weight loss.

For CG series samples, DTG curves showed the existence of C-S-H at 128 and 183 °C. Tiny characteristic peaks for Ht at ~350-380 °C were observed, which is consistent with the XRD results. It should be noted that the decomposition temperature of lead carbonate is less than 300 °C (Robin, 1996), which overlaps with that of C-S-H, obscuring its identification. The highest peak at ~440 °C is ascribed to the dehydration of portlandite, indicating its incomplete consumption during the slag activation process. The peak at ~657 °C is attributed to the emission of CO_2 from the calcium carbonate (CC), which was

resulted from the carbonation of portlandite. On the other hand, MG and MGPb1 pastes exhibited approximately the same DTG signs, namely, the broad C-S-H peak up to 250 °C, Ht peaks at around 370-380 °C, and 590 °C and CC peak at ~681 °C. The addition of Zn in the MG paste caused a significant change as manifested in DTG curve. Firstly, the peak for C-S-H diminished due to the retardation on the slag hydration. Secondly, the major decomposition temperature of Ht decreased slightly to around 343 °C and the peak at around 590 °C almost disappeared due to the substitution of Mg by Zn (Frost et al., 2003). Thirdly, it was observed that the peak intensity for CC decreased, which is ascribed to the retarded slag hydration and thus less carbonates as well as the incorporation of CO_2 into the Ht structure which released at lower temperature around 343 °C.

Combining the TG and DTG curves, the weight losses between 40 and 250 °C, denoted as Δm1 (mainly C-S-H), while the weight losses between 250 and 400 (for CG series), or 500 °C (for MG series), denoted as Δm2 (mainly Ht), were calculated and listed in Table 3. It can be seen that Zn significantly reduced the C-S-H content, while Pb only changed it slightly for both binders. Comparing the two binders, CG generated slightly more C-S-H than MG probably due to its higher pore solution pH and thus higher slag dissolution degree. The Ht content was significantly lower in CG series' pastes than in MG series' pastes and the effect of the Pb/Zn on the Ht content was marginal.

3.2. Strength development

It can be seen from Fig. 4a that even a small amount of Zn had a significant effect on the early strength of the mortars. After 28 d, the strength of Zn-doped samples decreased with the increase of Zn concentration, in which the 0.25% Zn-contained samples gained around 55% (~4 MPa) strength compared to the reference (CG). At 60 d, the strength of Zn-doped samples showed approximately the same strength and further curing only slightly increased

227 the strength, which is ~60% of the reference. The reduction of UCS by addition of Zn in the
228 lime-slag binder system was higher than that in the alkali-activated slag system as studied by
229 Deja (2002), which is attributed to the consumption of $Ca(OH)_2$ by the reaction with Zn,
230 resulting in a lower hydration degree of slag. On the other hand, the contanimation of Pb
231 caused a slight strength reduction in the short term (7 d), which was consistent with Rha et al.
232 (2000) and Hekal et al. (2012). After 7 d, the UCS of contaminated samples increased sharply
233 with curing time and exceeded that of the CG at 28 d when Pb concentration was over 0.5%.
234 After 160 d, samples with 0.5 and 1% Pb contamination gained approximately the same
235 strength, which were ~15% higher than the reference. Meanwhile, 0.25% Pb addition resulted
236 in a 12% reduction.

237 The MG series' samples performed quite differently in terms of UCS (Fig. 4b). In the
238 first two months, the UCS of the Zn-doped samples showed a steady increase although all
239 values were lower than that of the reference (MG). The reduction was dependent on Zn
240 concentration, with higher addition resulting in lower strength. After 160 d, the strength of
241 0.5% Zn-doped sample approached that of the reference while the others gained
242 approximately 70% and 65% of the control for the 0.25 and 1% Zn addition, respectively. As
243 for the Pb contamination, 1% Pb addition resulted in a higher strength than the reference in
244 the first month, while lower concentration exhibited nearly no influence on the UCS. After 60
245 d of curing, the reference samples showed higher strength than the Pb-doped samples, whose
246 strength decreased with the Pb concentration. After 160 d, reference samples only exhibited a
247 slightly higher strength than the Pb-doped samples, which is consistent with Deja (2002) that
248 lead showed no influence on the strength in the long term.

249 To compare the strength of both binders in the presence and absence of Pb or Zn, the
250 relative strength was calculated by dividing the strength values of MG series' samples by that
251 of the CG series' samples in each curing time. From Fig. 5, it was found that although MG

had lower early strength values, ~20% higher strength was gained after 60 d of curing compared to CG. This phenomenon was attributed to the lower pH value of MG system when activating GGBS at the early age, while more voluminous products (e.g., Ht, see Table 3) were formed to fill the pores during curing, resulting in higher strength in the long term.

For the Zn-doped samples, the significant effectiveness of MG system is illustrated in Fig. 5a, though this advantage over CG system was mitigated by the curing time. UCS after 7 d for CGZn pastes were approximately nil, which generated notably high relative values. After 28 d, the relative strength was from 1 to 7, increasing with the Zn concentration, while after 60 d of curing, the trend inversed, showing 30%~90% higher UCS in the MG system compared to the CG system, decreasing with Zn concentration. After 160 d, there was still 30%-65% higher UCS of MG series over CG series. The effect of Pb on the relative strength is shown in Fig. 5b. Samples with 0.25% Pb addition showed a similar trend as the reference samples, indicating the MG binder was more effective when treating low concentration of Pb contamination. However, when Pb concentration increased to 0.5 and 1%, the MG system showed lower UCS, but the difference was reduced with curing time, exhibiting only 5-10% lower strength than the CG system after 160 d.

3.3. Immobilisation efficiency

The immobilisation degrees were calculated using the immobilised fraction divided by the initial concentration in the binder. The leaching results and the immobilisation degrees of Pb and Zn by the CG and MG binders are shown in Table 4. For Zn contamination, MG binder was significantly more efficient compared to CG binder. After 7 d, the immobilisation degree decreased significantly for CG system with Zn concentration increased to 1% while that of MG system only decreased slightly. Increasing the curing time remarkably increased the immobilisation degree especially for high Zn contamination samples. CG paste achieved

over 99.95% immobilisation degree, which was only slightly lower than that of MG binder after 28 d of curing. As for Pb contamination, MG system was more efficient at early age with approximately all Pb immobilised regardless of Pb concentration. On the other hand, the immobilisation degree decreased slightly in CG system by increasing the Pb concentration from 0.25% to 1%. After 28 d, both binders fixed all the Pb. To compare, PC cured for 28 d was reported to have a Pb retention value of 99.82% and Zn retention value of 99.91% after leaching with deionised water when the initial metal/binder ratio was 1% (Giergiczny and Król, 2008). Clearly the binders in this study showed better immobilisation performance than PC as previously reported.

After leaching, the CG series' samples cured for 7 d showed pH values between 7.3-10.0. Leaching on the samples cured for 28 d gave pH values at 11.9-12.1. The increase of pH caused a higher leaching concentration for CGZn0.25 probably due to the re-dissolution of Zn compounds under high pH. While for CGZn1, the leached metal was significantly decreased due to a more mature hydration and the incorporation of Zn in the hydration products. On the other hand, pH values of MG series' samples were stable at 9.7-9.9 after 7 d of curing and slightly decreased to 9.6-9.7 after 28 d. As is known that pH has a significant effect on the solubility of the heavy metals, and most metal hydroxides have the least solubility at around pH 8.5-10.5 (Fernández et al., 2003). MG system proved to have better buffering capacity than CG system and the final pH value was within the range where most heavy metals have the minimal solubility, which is attributed to the higher content of Ht formed, as suggested in Jiang et al. (2007).

3.4. Microstructure

The SEM images for $Ca(OH)_2$-GGBS treated samples with 1% heavy metal addition cured for 28 d are shown in Fig. 6. The irregular GGBS particles bound by the C-S-H gels

and $Ca(OH)_2$ flakes were identified (Fig. 6a). The enlarged image (Fig. 6b) confirmed the presence of fibrous Ht and the EDS analysis showed that the point contained 3.23 wt% of Zn, which was much more than its overall concentration (1 wt%) indicating that a large portion of Zn has been incorporated in Ht. The Pb-doped $Ca(OH)_2$-GGBS pastes is shown in Fig. 6c and d. It appears that Pb-doped CG paste was featured by denser C-S-H gels, which agreed well with the UCS data. $Ca(OH)_2$ flakes were also detected and fibrous Ht were found to exist on the surface of the slag particle by a closer look (Fig. 6d). EDS point was pick on the agglomerate and showed the presence of Pb (Fig. 6e); however, due to its low content and the overlapping with Si, the quantification of the Pb content failed.

Significant difference was found between CG and MG samples doped with 1% Zn. SEM showed the prevalence of Ht in the matrix (Fig. 7a) agreeing well with the XRD and TG results. EDS analysis showed the point contained 1.36 wt% of Zn, which confirmed that a large portion of Zn has been incorporated in Ht considering the much larger content of Ht formed in MG pastes than in CG pasts (Table 3). Similarly, the Pb-doped MG paste showed a denser microstructure compared to Zn-doped paste (Fig. 7b). In addition, a few needle-like C-S-H was detected and a large amount of disintegrated agglomerates were observed which could be Pb-contained C-S-H agglomerates. EDS analysis showed the presence of Pb in these agglomerates although the quantification failed (Fig. 7c).

4. Conclusions

By investigating the hydration properties, strength development and immobilisation efficiency of slag activated by $Ca(OH)_2$ or reactive MgO in the presence of lead or zinc, the following conclusions can be drawn:

1. The main hydration products in both systems are C-S-H and hydrotalcite-like phases (Ht). Findings showed that the Ht played an important role in immobilising zinc

by incorporating it in its structure, while lead was primarily precipitated as hydroxide. Exposure to atmospheric CO_2 caused some degree of carbonation of the hydration products.

2. Lead retarded the early hydration of $Ca(OH)_2$ activated slag while the long term strength exceeded that of the control when lead concentration was over 0.5%. Zinc reduced the strength significantly by 40% after 160 d of curing regardless of the zinc concentration.

3. Both lead and zinc reduced the strength of reactive MgO activated slag, the extent to which depended on the metal concentration.

4. In terms of UCS, reactive MgO activated slag is more effective than $Ca(OH)_2$ activated slag in immobilising zinc regardless of the concentration and curing time. On the other hand, $Ca(OH)_2$ activated slag is preferable in treating higher level of lead contamination, though this advantage was mitigated by curing time.

5. The immobilisation degrees of lead and zinc were highly dependent of the pH and higher values were achieved by reactive MgO activated slag, which had increased buffering capacity due to the Ht formed and was able to maintain the pH value around 9.6-9.9 after leaching.

Acknowledgement

The authors are grateful to Cambridge Trust and China Scholarship Council (CSC) for their financial help of the PhD studentship for the first author.

References

Bankauskaite, A., Baltakys, K., 2014. The formation of different Mg–Al LDHs (Mg/Al = 2:1) under hydrothermal conditions and their application for Zn2+ ions removal. Sci. Sinter. 46, 95-106.

British Standards EN 196-1, 2005. Methods Of Testing Cement-Part 1: Determination Of Strength.

Deja, J., 2002. Immobilization of Cr6+, Cd2+, Zn2+ and Pb2+ in alkali-activated slag binders. Cem. Concr. Res. 32, 1971-1979.

Fernández, A.I., Chimenos J.M., Raventos, N., Miralles, L., Espiell, F., 2003. Stabilization of electrical arc furnace dust with low-grade MgO prior to landfill. J. Environ. Eng. 129, 275-279.

Frost, R., Martens, W., Ding, Z., Kloprogge, J.T., 2003. DSC and high-resolution TG of synthesized hydrotalcites of Mg and Zn. J. Therm. Anal. Calorim. 71, 429-438.

Giergiczny, Z., Król, A., 2008. Immobilization of heavy metals (Pb, Cu, Cr, Zn, Cd, Mn) in the mineral additions containing concrete composites. J. Hazard. Mater. 160, 247-255.

Harbottle, M.J., Al-Tabbaa, A., Evans, C.W., 2007. A comparison of the technical sustainability of in situ stabilisation/solidification with disposal to landfill. J. Hazard. Mater. 141, 430-440.

Hekal, E.E., Kishar, E.A., Mohamed, M.R., Mahmoud, M.K., Mohamed, B.A., 2012. Inertization of lead by using blended cement pastes. HBRC J. 8, 153-158.

Hosni, K., 2011. Using kaolinitic clay for preparation of a hydrotalcite-like compound. Mater. Sci. Appl. 2, 684-691.

Husillos Rodríguez, N., Granados, R.J., Blanco-Varela, M.T., Cortina, J.L., Martinez-Ramirez, S., Marsal, M., Guillem, M., Puig, J., Fos, C., Larrotcha, E., Flores, J., 2011. Evaluation of a lime-mediated sewage sludge stabilisation process. Product characterisation and technological validation for its use in the cement industry. Waste Manage. 32, 550-560.

Jiang, J., Xu, Y., Quill, K., Simon, J., Shettle, K., 2007. Laboratory study of boron removal by Mg/Al double-layered hydroxides. Ind. Eng. Chem. Res. 46, 4577-4583.

Jin, F., Gu, K., Abdollahzadeh, A., Al-Tabbaa, A., 2013. Effect of different reactive MgOs on the hydration of MgO-activated ground granulated blastfurnace slag paste. J. Mater. Civ. Eng. doi: 10.1061/(ASCE)MT.1943-5533.0001009.

Jin, F., Al-Tabbaa, A., 2013. Characterisation of different commercial reactive magnesia. Adv. Cem. Res. 26, 101-113.

382 Kogbara, R.B., Al-Tabbaa, A., 2011. Mechanical and leaching behaviour of slag-cement and
383 lime-activated slag stabilised/solidified contaminated soil. Sci. Total Environ. 409, 2325-
384 2335.

385 Kogbara, R.B., Yi, Y., Al-Tabbaa, A., 2011. Process envelopes for stabilisation/solidification
386 of contaminated soil using lime-slag blend. Environ. Sci. Pollut. Res. Int. 18, 1286-1296.

387 Liang, X., Zang, Y., Xu, Y., Tan, X., Hou, W., Wang, L., Sun, Y., 2013. Sorption of metal
388 cations on layered double hydroxides. Colloids Surf., A 433,122-131.

389 Park, M., Choi., C.L., Seo, Y.J., Yeo, S.K., Choi, J., Konarneni, S., Lee, J.H., 2007.
390 Reactions of Cu2+ and Pb2+ with Mg/Al layered double hydroxide. Appl. Clay Sci. 37, 143-
391 148.

392 Qian, G., Sun, D.D., Tay, J.H., 2003a. Characterization of mercury-and zinc-doped alkali-
393 activated slag matrix: Part II. Zinc. Cem. Concr. Res. 33, 1257-1262.

394 Qian, G., Sun, D.D., Tay, J.H., 2003b. Immobilization of mercury and zinc in an alkali-
395 activated slag matrix. J. Hazard. Mater. 101, 65-77.

396 Rha, C.Y., Kang, S.K., Kim, C.E., 2000. Investigation of the stability of hardened slag paste
397 for the stabilization/solidification of wastes containing heavy metal ions. J. Hazard. Mater. 73,
398 255-267.

399 Robin, J.H., 1996. Studies on the thermal decomposition of basic lead (II) carbonate by
400 Fourier-transform Raman spectroscopy, X-ray diffraction and thermal analysis. J. Chem. Soc.,
401 Dalton Trans. 3639-3645.

402 Rojas, R., 2014. Copper, lead and cadmium removal by Ca/Al layered double hydroxides.
403 Appl. Clay Sci. 87, 254-259.

404 Rötting, T.S., Ayora, C., Carrera, J., 2008. Improved passive treatment of high Zn and Mn
405 concentrations using caustic magnesia (MgO): particle size effects. Environ. Sci. Technol. 42,
406 9370-9377.

407 Roy, A., Eaton, H.C., Cartledge, F.K., Tittlebaum, M.E., 1991. Solidification/stabilization of
408 a heavy metal sludge by a Portland cement/fly ash binding mixture. Hazard. Waste Hazard.
409 Mater. 8, 33-41.

410 Scrivener, K.L., Kirkpatrick, R.J., 2008. Innovation in use and research on cementitious
411 material. Cem. Concr. Res. 38, 128-136.

412 Shand, M.A., 2006. The Chemistry And Technology Of Magnesia, John Wiley & Sons, New
413 Jersey, USA.

414 Spence, R.D., Shi, C., 2004. Stabilization And Solidification Of Hazardous, Radioactive, And
415 Mixed Wastes, CRC press, Bosa Roca, USA.

USEPA, 1992. Toxicity Characteristic Leaching Procedure, Test Method 1311, Washington, DC, USA.

Wang, S.D., Scrivener, K.L., 1995. Hydration products of alkali activated slag cement. Cem. Concr. Res. 25, 561-571.

Yi, Y., Liska, M., Al-Tabbaa, A., 2013. Properties and microstructure of GGBS-MgO pastes. Adv. Cem. Res. 26, 114-122.

Figure Captions:

Figure 1 XRD diffractograms of the MgO and GGBS used

Figure 2 XRD patterns for samples cured for 28 d (a) CG series; (b) MG series. Notation: C-S-H: calcium silicate hydrate; Ht: hydrotalcite-like phases

Figure 3 TG/DTG curves for samples cured for 28 d (a) CG series; (b) MG series.

Notation: C-S-H: calcium silicate hydrate; Ht: hydrotalcite-like phases; P: portlandite; CC: calcium carbonate

Figure 4 UCS development for mortar samples of (a) CG series; (b) MG series

Figure 5 Relative strength for references and (a) Zn-doped samples; (b) Pb-doped samples

Figure 6 Microstructural analysis of paste samples curing for 28 d: (a) and (b) SEM images of CGZn1 paste; (c) and (d) SEM images of CGPb1 paste and (e) EDS spectra of CGPb1paste

Figure 7 Microstructural analysis of paste samples curing for 28 d: (a) SEM images of MGZn1 paste; (b) SEM images of MgPb1 paste and (c) EDS spectra of MGPb1 paste

Table 1 Physico-chemical properties of the MgO, $Ca(OH)_2$ and GGBS used

Material		MgO	$Ca(OH)_2$	GGBS
Chemical composition (wt%)	MgO	93.2	-	8
	CaO	0.9	-	40
	$Ca(OH)_2$	-	96.9	-
	$CaCO_3$	-	1.4	-
	SiO_2	0.9	-	37
	Fe_2O_3	0.5	-	-
	Al_2O_3	0.22	-	13
	$Mg(OH)_2$	-	0.5	0.4
	Na_2O	-	-	0.3
	K_2O	-	-	0.6
	SO_3	-	0.02	2.5
LOI * (%)		2.6	-	1.4
Reactivity† (s)		100	-	-
BET surface area ($m^2\ kg^{-1}$)		9005	1529	493

* Loss on ignition † Measured by acetic acid test [21]

Table 2 Mix design for $Ca(OH)_2$-GGBS and MgO-GGBS samples

Mix denotation	Weight percentage in binder (%)			Metal (Zn/Pb) to binder ratio (%)
	$Ca(OH)_2$	MgO	GGBS	
CG	15	-	85	0
CGZn0.25	15	-	85	0.25
CGZn0.5	15	-	85	0.5
CGZn1	15	-	85	1
CGPb0.25	15	-	85	0.25
CGPb0.5	15	-	85	0.5
CGPb1	15	-	85	1
MG	-	15	85	0
MGZn0.25	-	15	85	0.25
MGZn0.5	-	15	85	0.5
MGZn1	-	15	85	1
MGPb0.25	-	15	85	0.25
MGPb0.5	-	15	85	0.5
MGPb1	-	15	85	1

Table 3 Calculated weight losses from TG curves of paste samples cured for 28 days

Mix denotation	Δm1 (%)	Δm2 (%)
CG	5.19	2.26
CGZn1	4.24	2.36
CGPb1	4.79	2.62
MG	4.62	5.74
MGZn1	3.13	5.36
MGPb1	4.61	6.00

Table 4 TCLP leaching results of the pastes after 7 and 28 days of curing

Mix denotation	7d			28d		
	pH	Leached metal (mg L^{-1})	Immobilisation degree (%)	pH	Leached metal (mg L^{-1})	Immobilisation degree (%)
CGZn0.25	9.96	0.062	99.95	11.88	0.264	99.79
CGZn0.5	7.26	0.356	99.89	12.14	0.220	99.91
CGZn1	8.68	93.67	81.27	11.89	0.178	99.96
CGPb0.25	9.44	ND *	100	11.66	ND *	100
CGPb0.5	9.52	ND *	100	11.86	0.072	99.97
CGPb1	8.82	0.369	99.93	11.86	0.18	99.96
MGZn0.25	9.72	0.060	99.95	9.58	0.091	99.93
MGZn0.5	9.70	0.054	99.98	9.55	0.082	99.97
MGZn1	9.80	0.118	99.98	9.56	0.076	99.98
MGPb0.25	9.91	0.027	99.98	9.66	0.066	99.95
MGPb0.5	9.88	ND *	100	9.65	0.062	99.98
MGPb1	9.83	ND *	100	9.64	0.166	99.97

* Not detected

Figure

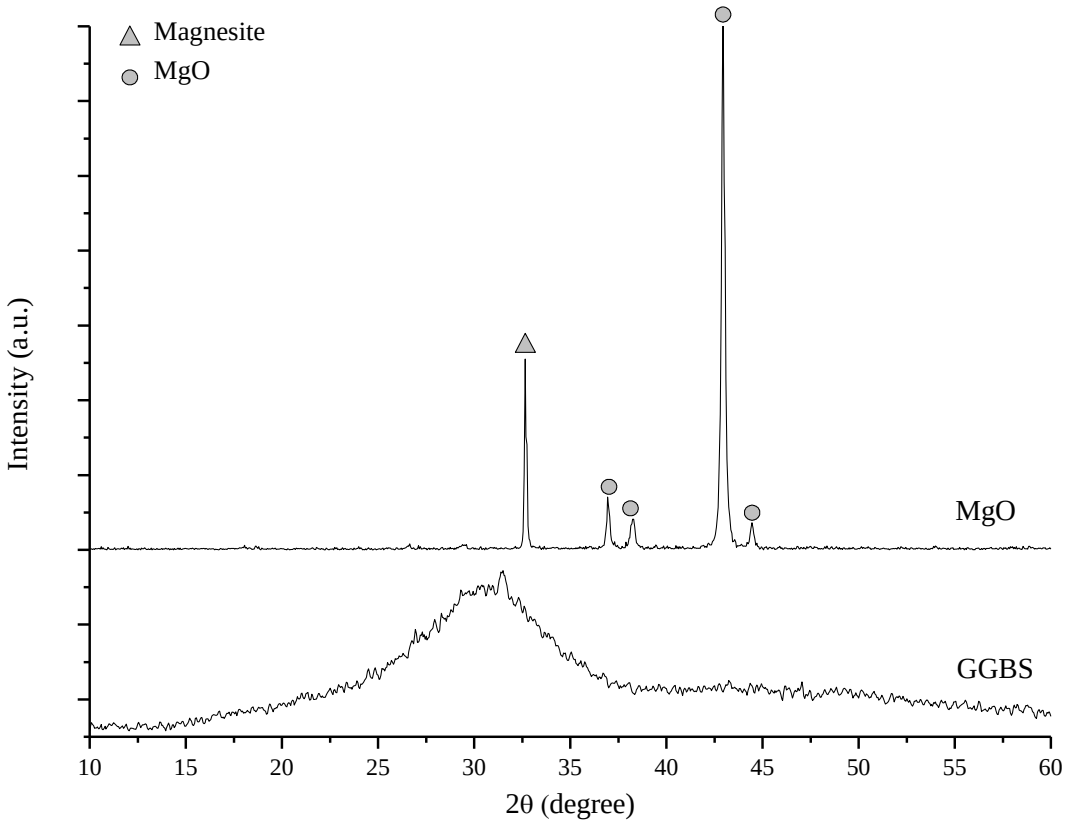

Figure 1 XRD diffractograms of the MgO and GGBS used

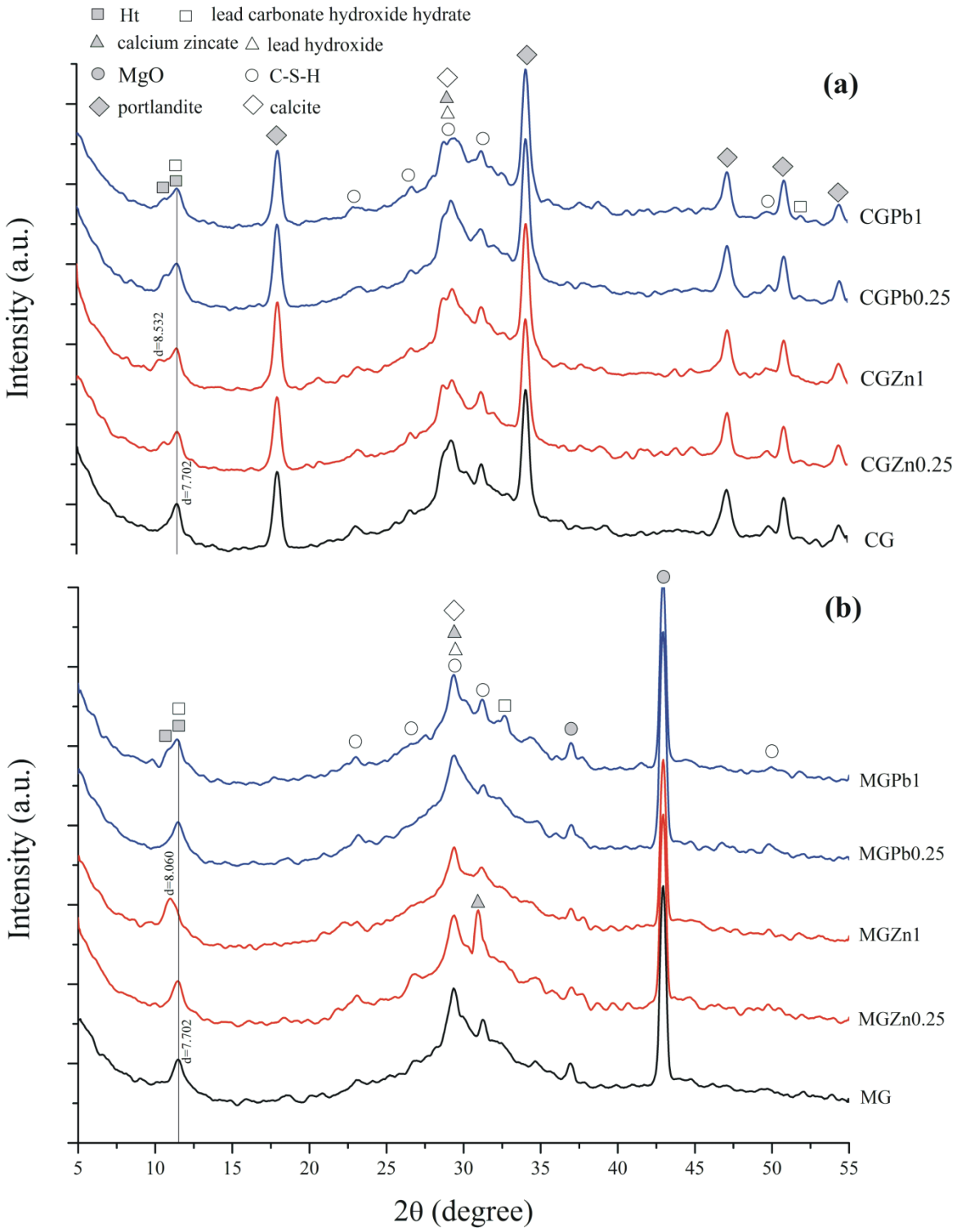

Figure 2 XRD patterns for samples cured for 28 d (a) CG series; (b) MG series. Notation: C-S-H: calcium silicate hydrate; Ht: hydrotalcite-like phases

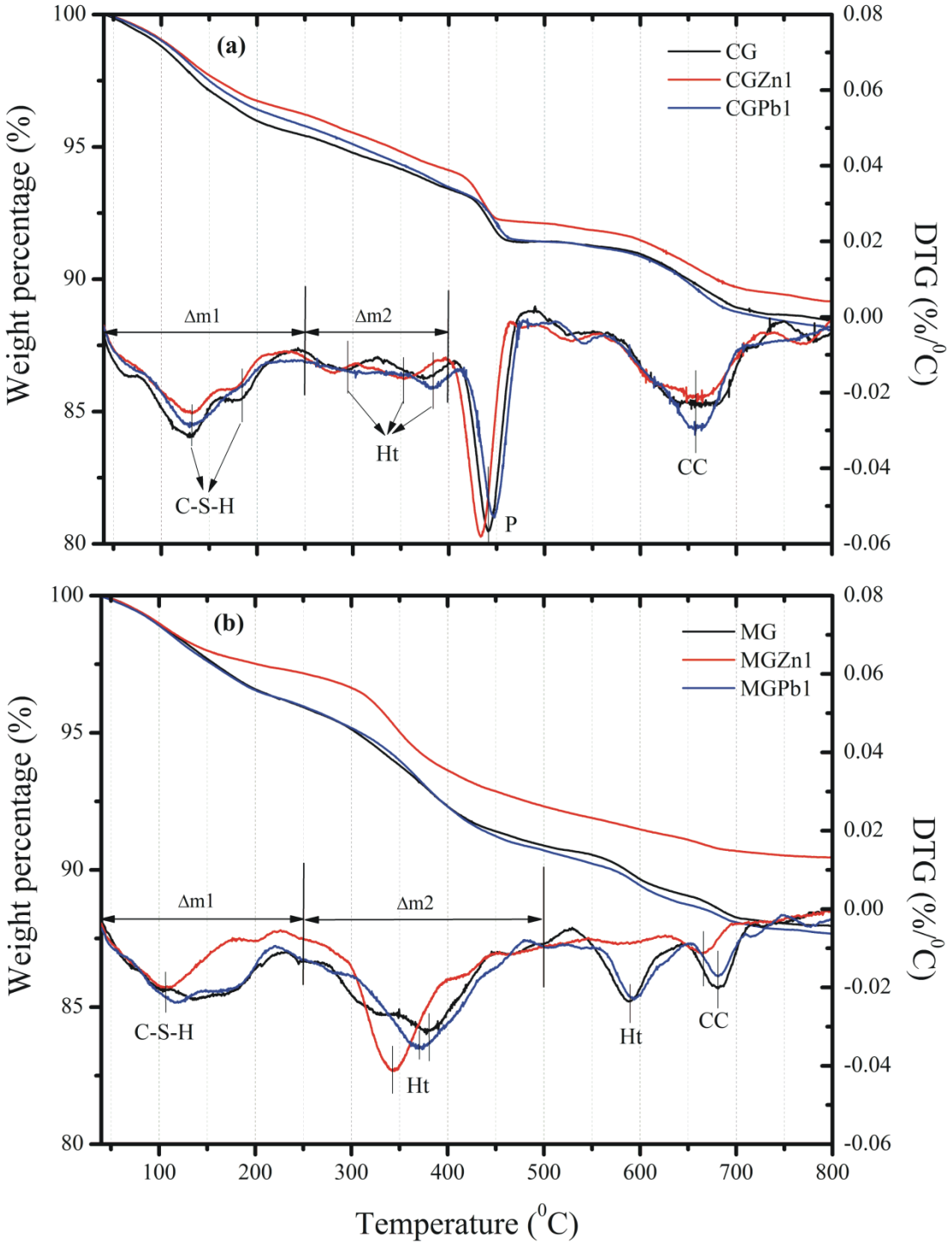

Figure 3 TG/DTG curves for samples cured for 28 d (a) CG series; (b) MG series.

Notation: C-S-H: calcium silicate hydrate; Ht: hydrotalcite-like phases; P: portlandite; CC: calcium carbonate

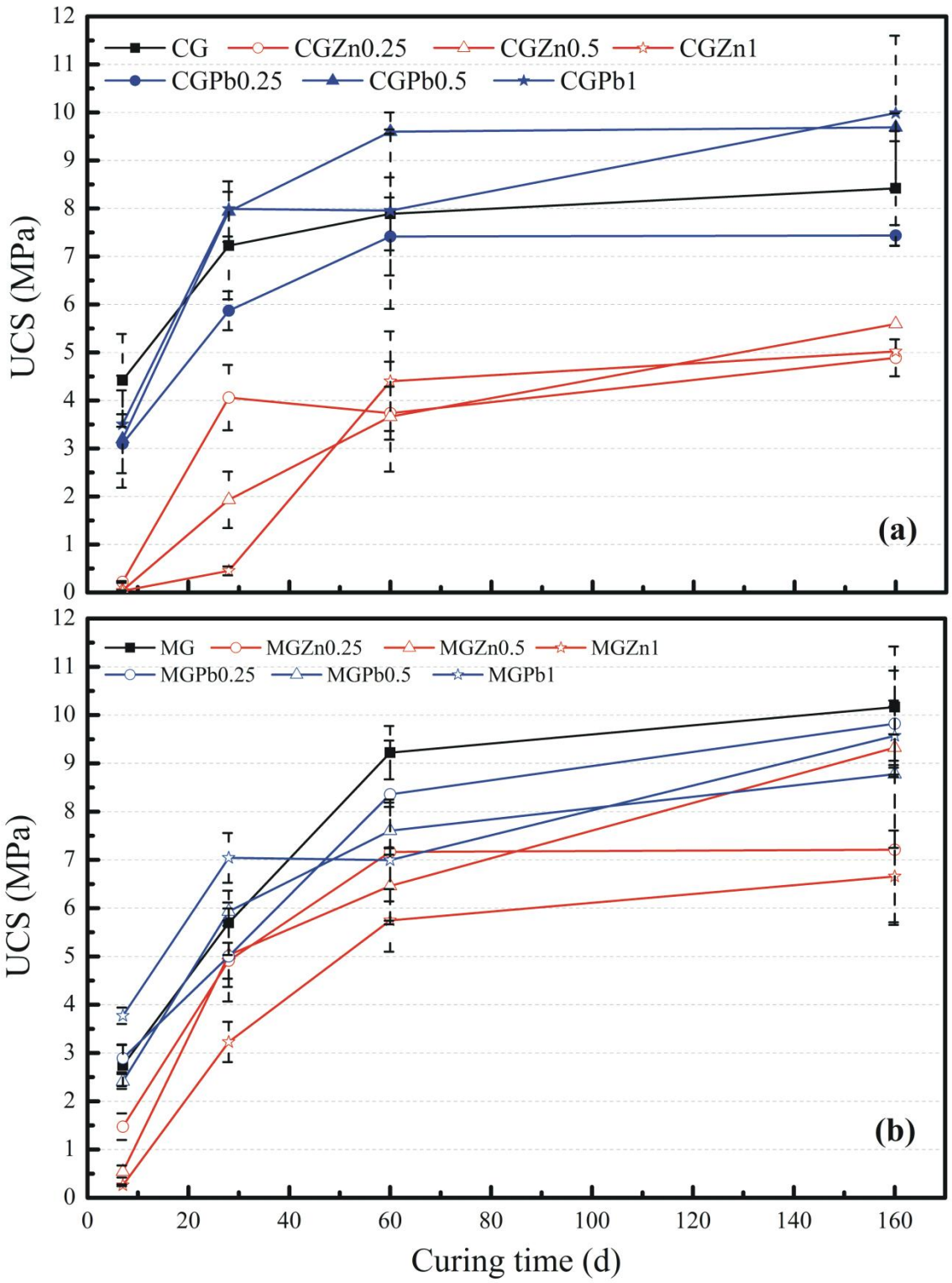

Figure 4 UCS development for mortar samples of (a) CG series; (b) MG series

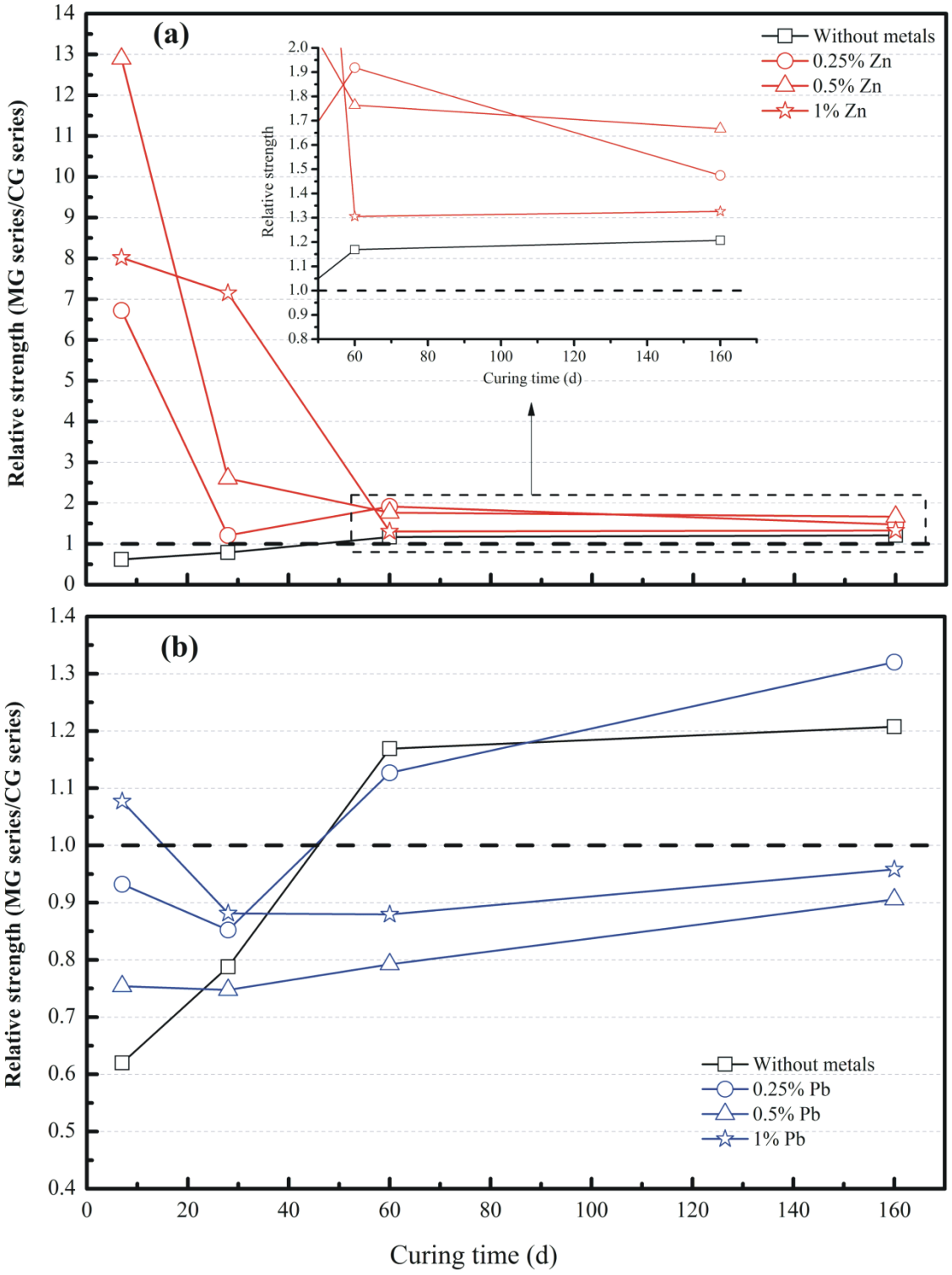

Figure 5 Relative strength for references and (a) Zn-doped samples; (b) Pb-doped samples

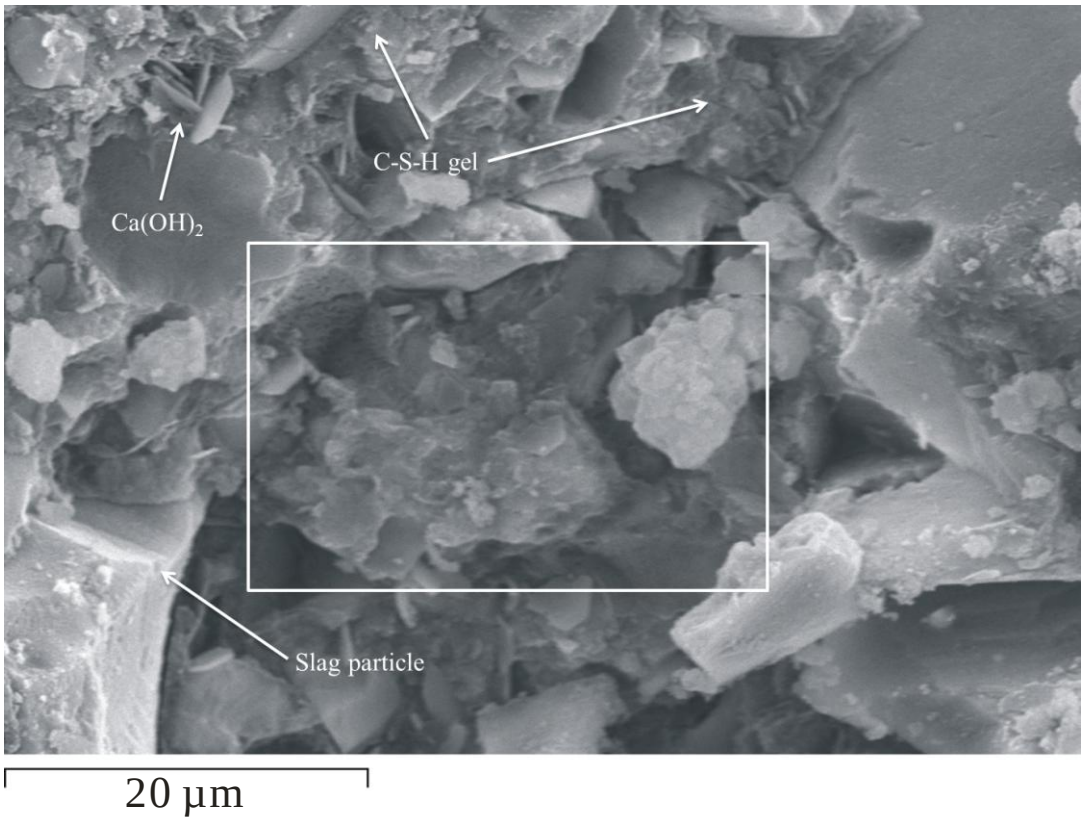
C-S-H gel
$Ca(OH)_2$
Slag particle
20 µm

(a)

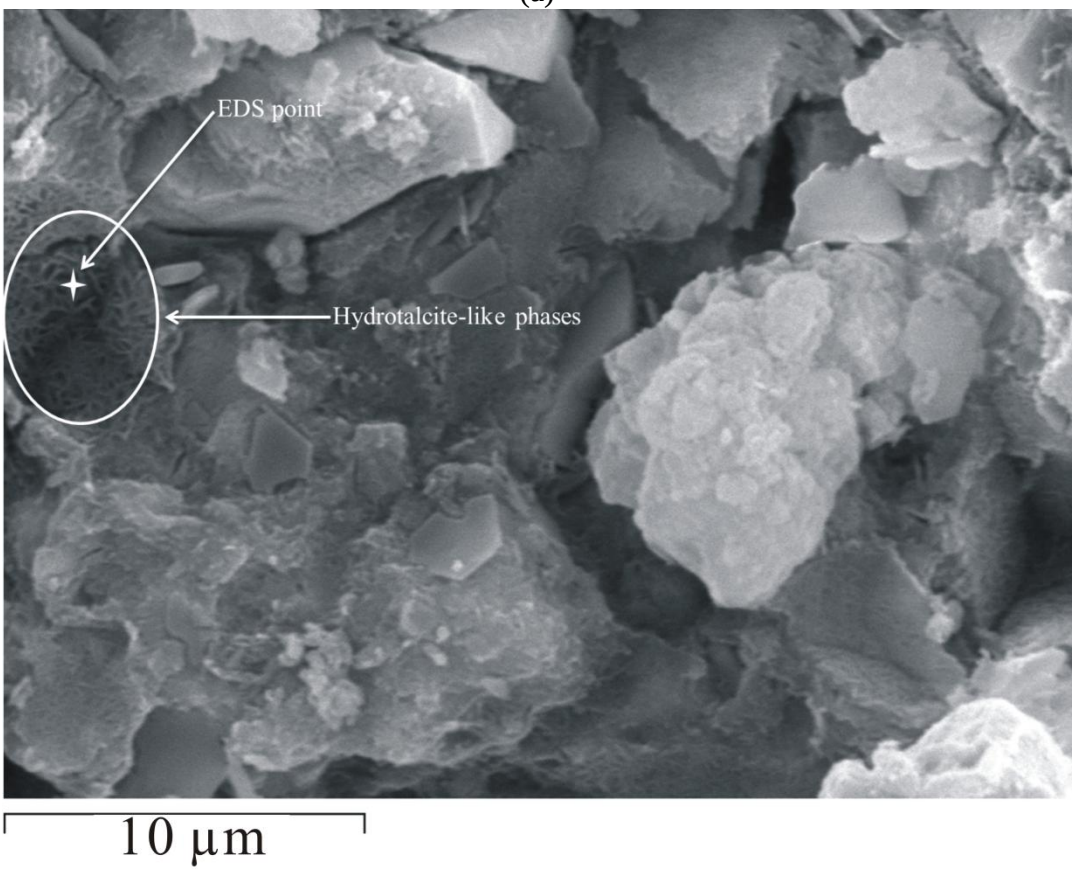
EDS point
Hydrotalcite-like phases
10 µm

(b)

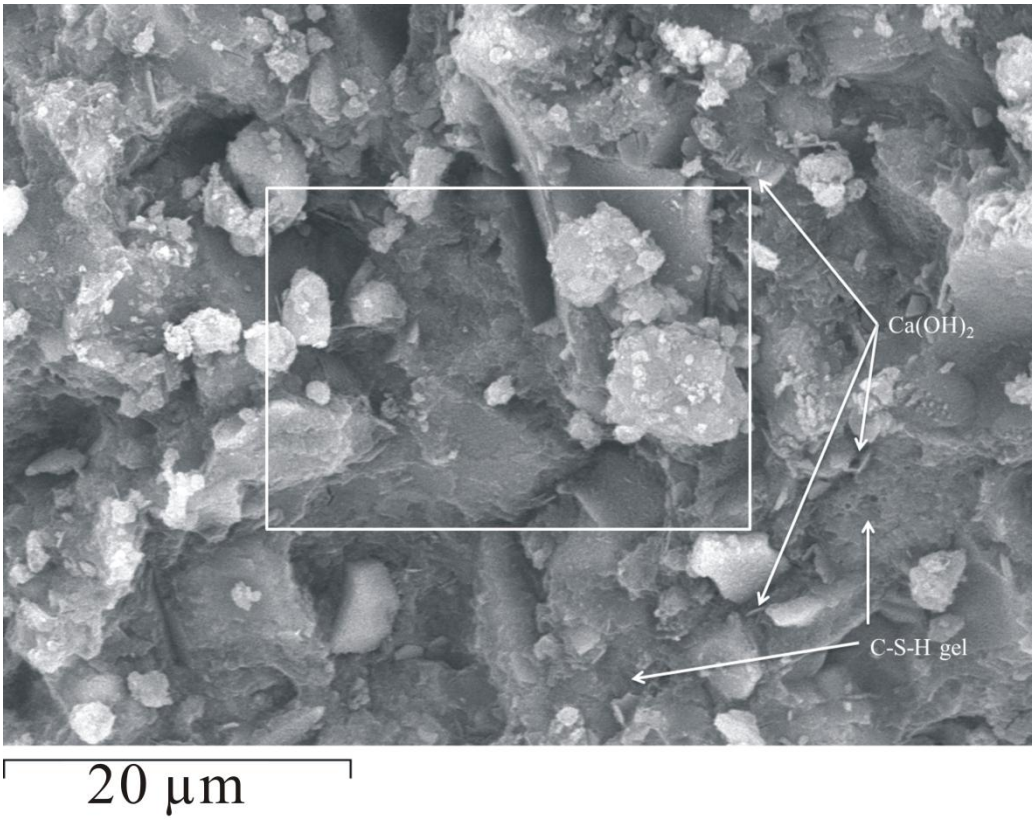

(c)

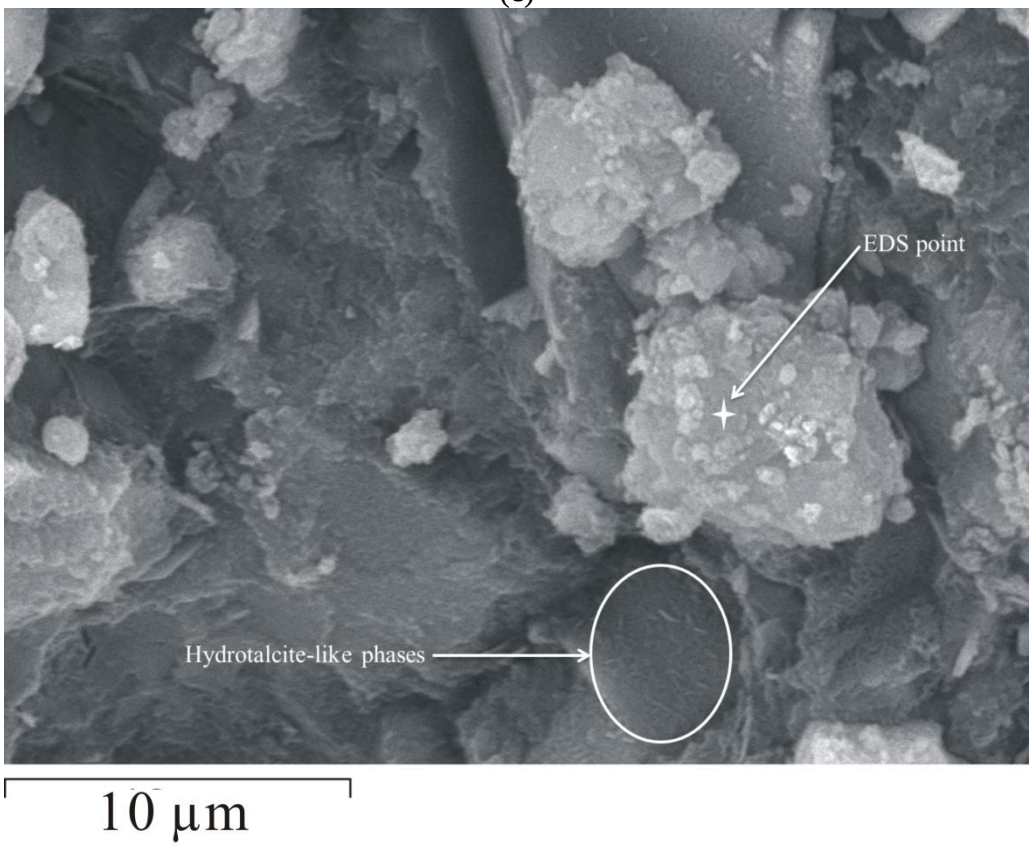

(d)

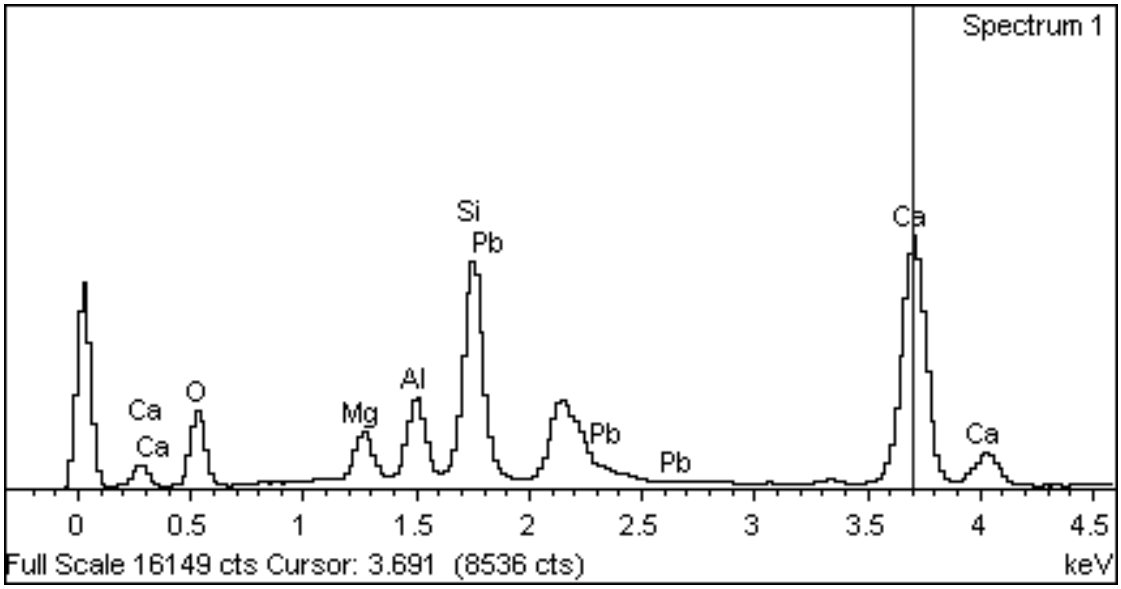

(e)

Figure 6 Microstructural analysis of paste samples curing for 28 d: (a) and (b) SEM images of CGZn1 paste; (c) and (d) SEM images of CGPb1 paste and (e) EDS spectra of CGPb1paste

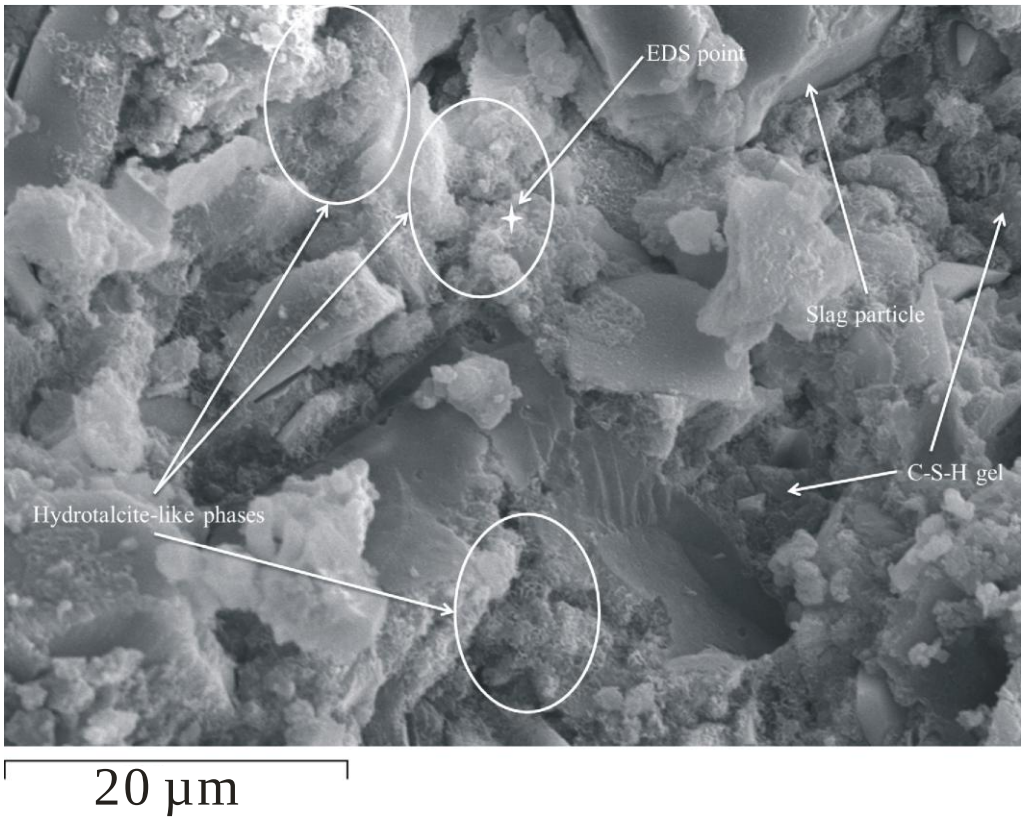
EDS point
Slag particle
C-S-H gel
Hydrotalcite-like phases
20 µm

(a)

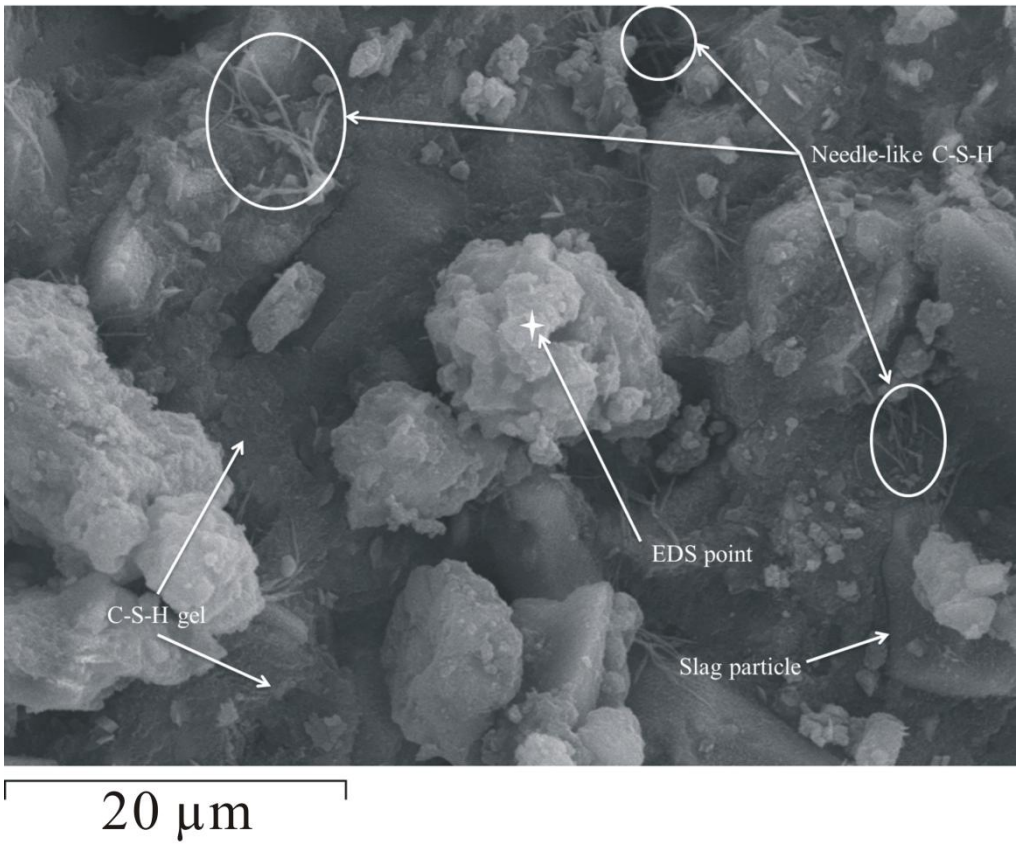
Needle-like C-S-H
EDS point
C-S-H gel
Slag particle
20 µm

(b)

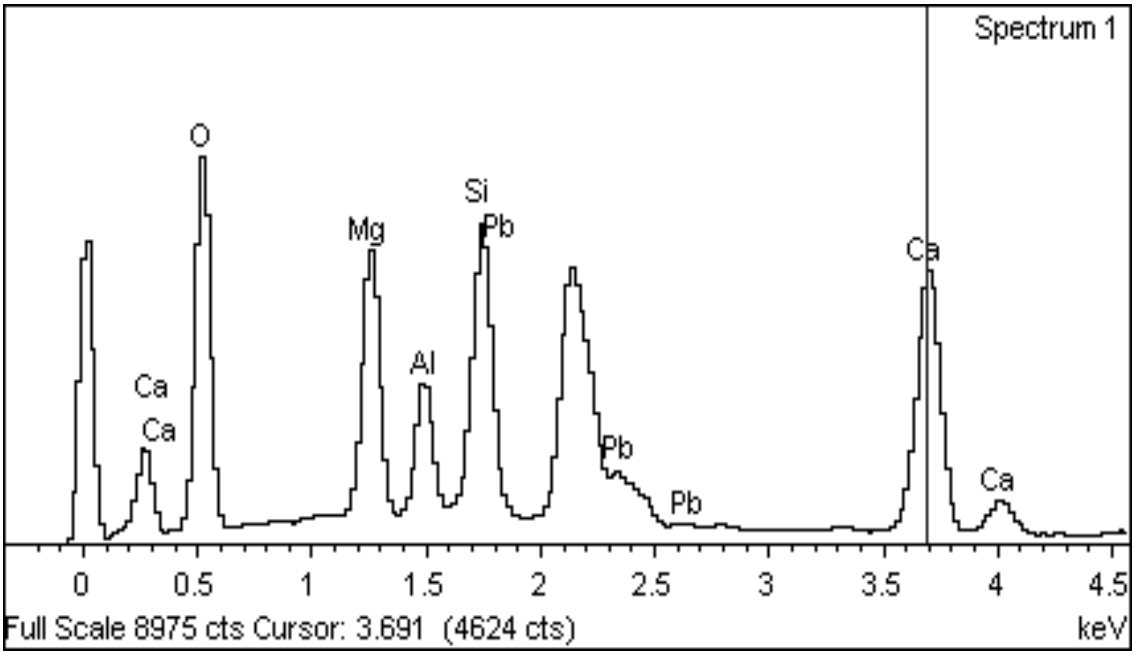

(c)

Figure 7 Microstructural analysis of paste samples curing for 28 d: (a) SEM images of MGZn1 paste; (b) SEM images of MgPb1 paste and (c) EDS spectra of MGPb1 paste